The Meteoritical Society

Meteoritics & Planetary Science 45, Nr 6, 947–964 (2010)
doi: 10.1111/j.1945-5100.2010.01068.x

A study of candidate marine target impact craters in Arabia Terra, Mars

Germari DE VILLIERS[1*], David T. KING JR.[2], and Luke J. MARZEN[2]

[1]Faculty of Geoscience, Universiteit Utrecht, Heidelberglaan 2, Utrecht 3584CS, The Netherlands
[2]Department of Geology and Geography, Auburn University, Auburn, Alabama 36830, USA
[*]Corresponding author. E-mail: g.devilliers@geo.uu.nl

(Received 11 May 2009; revision accepted 5 April 2010)

Abstract–Previous workers have proposed that a northern ocean existed early during Martian geologic history and the shorelines of that ocean would coincide roughly with the crustal dichotomy that divides the smooth, northern lowlands with the cratered, southern highlands. Arabia Terra is a region on Mars that straddles the crustal dichotomy, and several proposed shorelines are located in the area. Shallow marine impact craters on Mars likely would exhibit features like those on Earth, including characteristic morphological features that are distinctly different from that of craters formed on land. Common attributes of terrestrial marine impact craters include features of wet mass movement such as gravity slumps and debris flows; radial gullies leading into the crater depression; resurge deposits and blocks of dislocated materials; crater rim collapse or breaching of the crater wall; a central peak terrace or peak ring terrace; and subdued topography (an indicator of both age and possible flood inundation immediately following impact). In this article, these features have been used to evaluate craters on Mars as to a possible marine origin. This study used a simple quantification system to approximately judge and rank shallow marine impact crater candidates based on features observed in terrestrial analogs. Based on the quantification system, 77 potential shallow marine impact craters were found within an area bounded by 20°N and 40°N as well as 20°W and 20°E. Nine exemplary candidates were ranked with total scores of 70% or more. In a second, smaller study area, impact craters of approximately similar size and age were evaluated as a comparison and average total scores are 35%, indicating that there is some morphological difference between craters inside and outside the proposed shorelines. Results of this type of study are useful in helping to develop a general means of classification and characterization of potential marine craters.

INTRODUCTION

Impact craters are the most common physical features on most solid planetary surfaces in the solar system and are one of the most important physical features from which the evolutionary history and composition of these surfaces can be deduced. Crater studies can provide important information about the geologic history of planetary bodies in our solar system, and play a large role in understanding the properties of the target surfaces, their ages, and the physical conditions at the time of impact.

The physical conditions of planetary surfaces can be deduced from impact craters by looking at the morphology of these craters. One type of physical condition that is particularly important is surface water cover. A layer of water on the surface influences the shape of the final crater (Gersonde et al. 2002; Ormö et al. 2002), and thus the morphology of craters formed in subaerial environments differs from that of craters formed in submarine environments. This study explored the surface in an area on Mars previously suggested to be a shallow continental shelf environment (e.g., Parker et al. 1989; Edgett and Parker 1997; Clifford and Parker 2001; Fairén et al. 2003; Ormö et al. 2004) by investigating Martian craters in that area, which may have formed in such a shallow marine environment. Although it is believed that marine target craters should

Table 1. Marine impact craters on Earth. Modified from Ormö and Lindström (2000) and Dypvik and Jansa (2003). The five impact craters that are primarily used as analogs in this study are printed in italics.

Crater	Locality	Diameter (km)	Age (Myr)
Avak	Alaska, USA	12	>95
Chesapeake Bay	*Virginia, USA*	*85*	*35.5 ± 0.3*
Chicxulub	*Yucatán, Mexico*	*~180*	*64.98 ± 0.05*
Eltanin	South Pacific	?	2–15
Gusev	Donets, Russia	3	49.0 ± 0.2
Granby	Linköping, Sweden	3	470
Kaluga	Kaluga, Russia	15	380 ± 5
Kamensk	Donets, Russia	25	49.0 ± 0.2
Kara	Kara Sea, Russia	65	70.3 ± 0.3
Kärdla	Hiiumaa, Estonia	4	455
Karikkoselkä	Läsi-Suomi, Finland	1.3	440–445
Lockne	*Östersund, Sweden*	*13.5*	*455*
Mjølnir	*Barents Sea, Norway*	*40*	*142 ± 2.6*
Montagnais	Nova Scotia, Canada	45	50.5 ± 0.76
Neugrund	Gulf of Finland, Estonia	20	535
Ust Kara	Kara Sea, Russia	25	70.3 ± 2.2
Wetumpka	*Alabama, USA*	*7.6*	*81.0 ± 1.5*

exist on Mars and some craters have been identified previously as potential shallow marine impact craters (Ormö et al. 2004), as yet there is still no catalog of potential marine crater candidates and large areas of continental shelf environment lie unexplored.

The influence of the target material composition is a common topic of research in impact studies and it may even be more important in shape determination than the properties of the projectile (Melosh 1989). Observations of Earth-based marine target impacts as well as numerically modeling, show that the water column greatly influences the shape, size, and lithology of the resulting crater fill (Gersonde et al. 2002; Ormö et al. 2002, 2004; Senft and Stewart 2007). This gives impacts into marine environments a substantially different appearance from impacts into dry, subaerial targets. Impacts into sedimentary targets where sediments overlie basement rock generally exhibit two-fold rheology: a weak, volatile-rich upper layer, and a hard, crystalline lower layer. Impacts into soft, layered targets, such as unconsolidated sands, yield craters that are commonly larger, than impacts into solid targets such as crystalline bedrock, because of the differences in strength of the various layers that are present in the target material (Ormö and Lindström 2000; Ormö et al. 2002; Kenkmann and Schönian 2005; Senft and Stewart 2007). However, if the crater target materials are in turn overlain by a layer of water, the three-layer composition makes the morphology of the resulting crater even more specific, commonly resulting in an ''inverted sombrero'' shape (Collins and Wünneman 2005; Horton et al. 2005, 2006; Kenkmann and Schönian 2005). This inverted sombrero shape is an outer ring with a large, inward-sloping, annular surface surrounding a central uplift or central ring uplift, which may have a deeper inner crater within. In this scenario, the target rheology is also responsible for creating planes on which slump blocks can easily slide down, resulting in a larger crater with a wider annular trough (Collins and Wünneman 2005; Senft and Stewart 2007). This is a combined effect of the target being saturated and the water returning (either as a flow or as moving pore water exerting pressure).

Even though few marine impact craters are identified on Earth, it should be noted that exceptional preservation is required to confirm marine origin. When seafloor craters are formed, their postmodification shapes are usually better preserved in aqueous environments because of rapid sediment burial preserving the shape of the crater (Ormö and Lindström 2000; Dypvik et al. 2004), hence most confirmed marine impacts are well-preserved examples. Table 1 lists the locations, diameters, and ages of 17 confirmed marine impact craters on Earth. This study focused on craters within a size range of 10–100 km in diameter. The spatial resolution of the topographic data determined the lower limit, whereas the upper limit is really an arbitrary cut-off. Note that most of the terrestrial analogs for shallow marine impact craters fall within this range.

The selected area of study on Mars falls largely within northwestern Arabia Terra (NWAT) with small sections in Acidalia Planitia and Chryse Planitia. The study area lies just above the equator on the central meridian line and is bounded by the 20°N and 40°N latitude lines as well as the 340°E and 20°E longitude

lines. Arabia Terra is a large, flat region that straddles the crustal dichotomy. Average elevation is approximately 1–2 km below mean surface level. The study area comprises mainly the Noachis Terra geological unit which is Noachian in age (Tanaka et al. 2005). Two smaller geological units, Nepenthes Mensae (of Early Hesperian to Early Noachian age) and Vastitas Borealis (of Amazonian age) are also present within the study area (Tanaka et al. 2005). However, the fact that Arabia Terra is covered by a thin layer of fine-grained sand or silt does not mean that it had to have been covered in water. It could have been volcanic (e.g., Hynek et al. 2003) or aeolian (e.g., Fassett and Head 2007). For the purpose of this study, assuming that a large sea once covered the northern lowlands early in its history (e.g., Parker et al. 1989; Clifford and Parker 2001; Fairén et al. 2003), water would have covered all areas north of the dichotomy, thus creating a shallow water, continental shelf environment of varying width all along the dichotomy, may be on more than one occasion. On Earth, a continental shelf is an ideal setting for the preservation of shallow marine impact craters because a seafloor crater is more likely to form in shallow water and in this setting rapid sedimentation is more likely to keep further erosional processes from destroying the crater geomorphology. Therefore, NWAT, which arguably could once have been part of a continental shelf, makes a suitable study area for shallow marine impact craters.

BACKGROUND

According to Artemieva and Shuvalov (2002), when a projectile enters an aqueous target there are numerous events that occur in the water column and on the seafloor, including a strong shock-wave, surge formation, and tsunamis. Sonett et al. (1991) have done both numerical and laboratory studies on impacts into oceanic environments and conclude that there are at least two strong waves generated upon impact, which can be responsible for surge and resurge formation as well as tsunamis. These events, combined with the stages of crater formation (contact and compression, excavation, and modification; Melosh 1980), are used to formulate an idea of which target morphologies can be expected in shallow marine craters.

Good terrestrial analogs formed in a continental shelf environment show well-preserved structures and features that are commonly preserved in detail. Some analogs were particularly useful in this study, and they include the large Chesapeake Bay impact structure (CBIS; Horton et al. 2006) and Chicxulub (Collins et al. 2002) craters, the medium Lockne (von Dalwigk and Ormö 2001) and Mjølnir (Gudlaugsson 1993; Dypvik et al. 1996) craters, as well as the small Wetumpka crater (King et al. 2002; Table 1).

CBIS, currently buried beneath 150–400 m of postimpact sediments (Horton et al. 2006), is very well preserved but not visible from the surface. Collins and Wünneman (2005) modeled the Chesapeake impact event and concluded that the main factor responsible for the morphology of the crater is the variation in strength of the layers present in the target. Without this variation in strength among the layers, it is likely that the diameter of the Chesapeake structure would have been only half of the actual 85 km determined through seismic profiling (Collins and Wünneman 2005). CBIS crater exhibits "inverted sombrero" morphology and the rim has been subject to large-scale collapse and slumping resulting in crater-wall failure (Poag 1997; Horton et al. 2006). Numerous extensional collapse structures are observed in the seismic profiles, resulting in radial enlargement of the crater (Poag 1997; Horton et al. 2006). Chicxulub crater is well preserved beneath a layer of sediments and the surge deposits are particularly well preserved, including deposits of massive sands, debris flows, and collapse of the central peak into a peak ring (Dypvik et al. 2004; Kring 2005). Lockne crater contains very good examples of resurge gullies that have been associated with large-scale resurge flows (von Dalwigk and Ormö 2001). Four gullies, as well as a few debris flow units, have been described and the rim has been classified as breached in more than one location (von Dalwigk and Ormö 2001). Mjølnir crater is not exposed at the surface, but instead is located on the seafloor and presently covered by approximately 350 m of water and 50–400 m of sediments (Gudlaugsson 1993; Dypvik et al. 1996; Dypvik and Jansa 2003). The Mjølnir crater rim is characterized by terraces that are bordered by faults and possible gullies (Dypvik and Jansa 2003). This crater also exhibits the classic inverted sombrero morphology with inner and outer zones (Dypvik and Jansa 2003) and rotated fault blocks are found in the annular trough (Ormö and Lindström 2000). Wetumpka crater exhibits signs of intracrater and extracrater resurge deposits (RD) as well as a partially collapsed rim (King et al. 2002, 2006), which provided an avenue of marine resurge into the crater.

Based on the morphological characteristics observed in the terrestrial analogs mentioned before, several indicative characteristics that can be associated with shallow marine impact craters have been identified. These include features indicative of wet mass movement (WMM; Dypvik et al. 2004), radial gullies (RG; von Dalwigk and Ormö 2001), RD, collapsed rims, central

terraces (CT), and subdued topography (ST; see de Villiers et al. 2007). These features are visible in high resolution orbital images and could therefore be used as key characteristics in the identification of Martian shallow marine impact craters.

Wet Mass Movement

WMM occurs when saturated sediment is mobilized, either in a brittle or ductile manner (Dypvik and Jansa 2003). Mass movement can occur at various rates, but most important in this study is the rapid movement of unconsolidated sediment as a result of weakness induced by saturation. Two types of mass movement are particularly important: slides, where the movement occurs in a well-defined plane; and flows, where the movement is more fluid in behavior and of which the deposit shape is more rounded and continuous. A slump is a brittle slide where material moves downward as a parcel or unit, often with a backward rotation on a curved displacement surface (Kennett 1982). Listric or normal faults form as the result of this displacement. A debris flow is a ductile flow where particles chaotically move down slope in water-saturated sediment slurries while supported by cohesion strength (Kennett 1982). Slumps, or block collapse of rim material into the crater are indicative of weak or unconsolidated target material (Dypvik and Jansa 2003). Slump blocks are present in both Mjølnir and Chesapeake Bay crater structures (Ormö and Lindström 2000) and slump flows, have been observed in both Chicxulub (Kring 2005) and Lockne (von Dalwigk and Ormö 2001) craters.

Radial Gullies

Resurge channels carved by sediment-loaded waters induced by violent floods are common in marine-target craters (Ormö and Muinonen 2000; von Dalwigk and Ormö 2001). RG have been observed in both the Lockne (Lindström et al. 1996) and Kamensk (Ormö and Lindström 2000) craters. Even though resurge gullies are expected to be one of the most distinctive characteristics of marine impact craters, they tend to occur only in deeper water where the water depth exceeds the projectile diameter (Ormö et al. 2002), hence are not expected to be that common in Arabia Terra, unless the shorelines were much higher than currently envisaged. The water depth at the time of impact for Lockne has been estimated at 1000 m (Ormö et al. 2002) and for Kamensk at 100–200 m (Ormö and Lindström 2000)—clearly very shallow water depths limit the potential for the formation of RG.

Resurge Deposits

Deposits related to surge or resurge flows may form inside or outside of the crater, depending on the depth of the target water, the strength of the target material, and possibly the location of the crater with respect to the main direction of surge flow (Ormö et al. 2007). Intracrater terrain is the evidence of surge in the form of avalanches, slides, and slumps of mixed blocks inside the crater (Dypvik and Jansa 2003). Extracrater terrain is the evidence of surge in the form of resurge sediments and mixed blocks outside the crater (Dypvik and Jansa 2003). As discussed by King et al. (2006), the "extrastructure terrain" observed at Wetumpka is likely a product of collapse of the rim in respond to flow. RD are more often aqueous debris flows and not slump blocks. RD on Earth have been confirmed through drilling and fieldwork in combination with subsequent sedimentological description (von Dalwigk and Ormö 2001; King et al. 2006), but may be difficult to discern from satellite imagery. Because of the directional relationship between these two types of deposits and their depositional agents, they are kept in the same category and not grouped with features of WMM.

Rim Collapse (RC)

Crater rims are usually tough features formed from crystalline bedrock. When craters form in sedimentary environments, the rims are not as pronounced or as strong. Often no remnant of rim is visible because of large amounts of inward slumping (Dypvik and Jansa 2003). This is sometimes also referred to as structural rim failure. Structural rim failure may be a result of the instability of the rim or because of resurge activity (King et al. 2006). In fact, collapsed rims are usually associated with WMM and resurge (Dypvik and Jansa 2003). However, WMM can occur without a breach in the rim and is also observed without the presence of identifiable gullies.

Central Terrace

A central peak terrace or a peak ring terrace is a large structure in the center of the crater, sometimes associated with equally flattened concentric rings (Dypvik and Jansa 2003). In smaller craters, a central pit (most likely the summit pit-type) may be present instead of a peak ring (Barlow 2010). Development of flat-topped central uplifts has been predicted by some studies (Gault and Sonett 1982) and could be an indication of marine origin and that the structure has been buried under water for some time. CT indicate long-standing water, potentially spanning from right

after formation until the end of the oceanic phase (Gault and Sonett 1982; Dypvik and Jansa 2003).

Subdued Topography

Craters that exhibit ST have little to no elevation of the rim above the surrounding topography. ST is indicative of the amount of erosion that has taken place since formation, and thus the amount of time that has passed. As erosion is often induced by water, it could also indicate that large amounts of water were present on the surface for an extended period of time (Ormö and Lindström 2000). If an ocean once existed in the northern lowlands on Mars, it could have occurred during the late Noachian, very early in Mars' history (Parker et al. 1989; Fairén et al. 2003), leaving plenty of time for the craters to become degraded and the surrounding topography to become subdued. Lack of an elevated rim is considered by Dypvik and Jansa (2003) to be one of the most distinctive features of marine impacts, yet it could also merely indicate age.

Note that none of the characteristics listed before can be used with certainty to imply marine origin. Other processes may be responsible for generating similar features in different locations; for example, complex craters on Earth often show signs of slumping without having formed in marine environments. Only evidence of deposition of marine sediments before and after the impact event, or drill cores proving the existence of resurge deposits, is conclusive evidence. However, if more than two of these geomorphic characteristics are observed, it is more likely that a marine origin can be implied.

METHODS

This study employed data sets gathered by three different instruments: (1) Mars Orbiter Laser Altimeter (MOLA) and (2) Mars Orbital Camera (MOC), which were onboard the Mars Global Surveyor (MGS) spacecraft, and (3) Thermal Emission Imaging System (THEMIS) onboard the Mars Odyssey spacecraft. The spatial resolutions of these data sets are substantially better than that of the Viking images, which previously were used in areomorphological studies of this nature. MOC images are generally at 2–10 m per pixel resolutions when taken with the narrow angle camera (Malin et al. 1992) and THEMIS visual imagery generally have resolutions of around 20 m per pixel (Christensen et al. 2004). For topography, a MOLA 128 m per pixel base map from the Planetary Data System was downloaded.

All the expected characteristics listed above were observed, including (1) evidence of WMM; (2) RG entering the crater from one or more location on the crater rim; (3) RD; (4) evidence of RC; (5) CT; and (6) ST (examples shown in Fig. 1). From these observed features, six categories were constructed in a database of potential marine target craters, including WMM, RG, RD, RC, CT, and ST. These categories were weighted to reflect relative importance of various characteristic features. WMM is an important, relatively indicative factor, and as such comprises 40% of the score. This includes 20% for evidence of slumping and 20% for evidence of debris flows. RG, although not as common in shallow water as in deeper water, is also indicative and therefore comprises a further 20% of the score (one gully is 10%, and two or more gullies is 20%). RD are more difficult to discern from orbital imagery, resulting in the factor only comprising of 10% of the score. RC, CT, and ST are all factors that are less indicative of marine origin, or not necessarily related to marine origin, and thus make up only 10% each of the total score. Weight distributions for these characteristics are shown in Fig. 2. WMM is likely the most important characteristic, however, it should be noted that there are numerous ways of forming WMM features and that these features do not only occur in shallow marine environments.

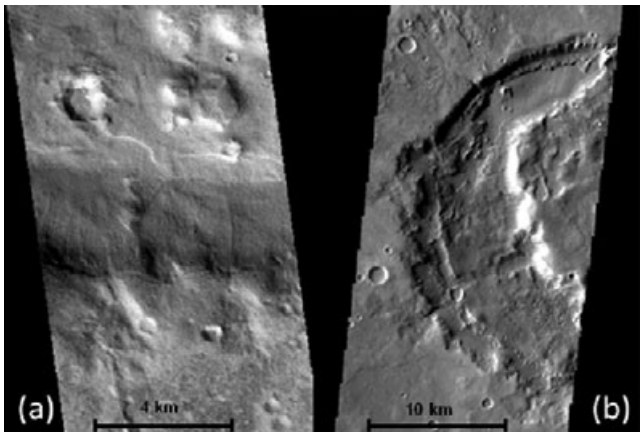

Fig. 1. Examples of subdued topography and no elevated rim (a) (Mars Orbital Camera image E0600102 located at 39°N; 359°E); as well as a central terrace and possible resurge deposits (b) (Thermal Emission Imaging System image V12594005 located at 39°N; 11°E).

This system makes it possible to approximately quantify the features observed and to rate each crater based on properties associated with terrestrial marine craters. Each candidate crater is assigned a total score and these values are used to rank and classify shallow marine crater candidates.

RESULTS

Four sets of analyses were performed: (1) a pilot analysis on earlier identified candidates to act as

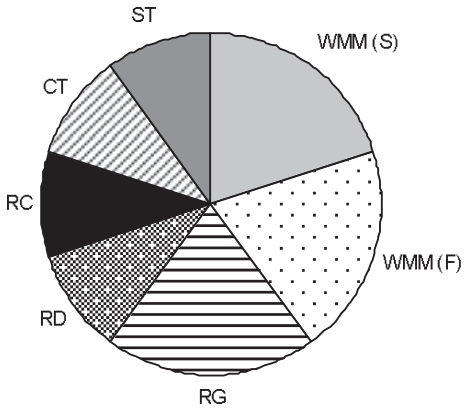

Fig. 2. Weighted distribution of the six classes of shallow marine crater characteristics including: wet mass movement (WMM), radial gullies, resurge deposits, rim collapse, central terrace, and subdued topography. Note that WMM is split into two subcategories (S, slump; F, flow).

reference for subsequent sets; (2) an initial analysis based on available MOC imagery for the study area (set A); (3) a second analysis based on MOLA topography (set B); and (4) a comparative analysis in an area slightly southeast of the Arabia Terra study area. The pilot analysis was performed on the potential craters proposed by Ormö et al. (2004). All the results of the ratings for the first three sets are given in Table 2. Results of the comparative analysis are given in Table 3. All the crater candidate sites fall north of (within) the Meridiani shoreline (shown in light gray on Fig. 3) proposed by Edgett and Parker (1997) and discussed by Fairén et al. (2003), and only a few fall north of (within) the Noachian Arabia shoreline (original contact 2—shown in white; Parker et al. 1989; Fairén et al. 2003). The Deuteronilus shoreline (Parker et al. 1989; Fairén et al. 2003) is likely the result of a smaller, more recent Hesperian ocean and is indicated in dark gray. The location of this shoreline is largely outside the study area, which is indicated by the gray rectangle and can be seen to encompass a large part of the Arabia Terra continental shelf.

Ormö et al.'s Candidate Crater Results

The four craters proposed by Ormö et al. (2004) as potential shallow marine impact craters were rated first in the quantification system. The assigned total value is a number ranging from 0.0 to 1.0, reflecting the percentage confidence that a particular crater is of marine origin. A stacked histogram is plotted with all the variables shown as individual blocks (Fig. 4). Total scores range from 0.5 to 0.8 as even these prime examples do not exhibit all possible characteristics. Crater D is the most likely of the marine impact crater candidates proposed by Ormö et al. (2004) to be a shallow marine impact crater with an assigned total score of 0.8. Five of six categories have features present in crater D, and both slumps and flows are observed.

Results from Set A

In the database of MOC images in Arabia Terra there are 868 images that were taken during the period from September 1997 to September 2005. Through thorough screening, 51 images of 40 candidate craters were identified as useful. Pertinent THEMIS images were subsequently downloaded for the 40 candidate sites to serve as context images.

Fifteen of the candidate craters were found to be too small (diameters < 10 km) to fall within the population for this study and were thus discarded. The 25 remaining craters were divided into three groups based on size. These divisions were created because the size of the crater could affect the morphology of the crater (Dypvik and Jansa 2003), and as such an effective assessment of craters can only be done if similar craters are compared with each other. Small craters have diameters of 10–30 km, medium craters have diameters of 30–50 km, and large craters have diameters of 50–100 km. These 25 shallow marine crater candidates were rated for shallow marine origin and plotted in Fig. 4, with the craters clustered based on size. The first 20 craters are small (D = 10–30 km), the next four are medium (D = 30–50 km), and the last one is large (D = 50–100 km). It is evident from the data that the population is skewed to the smaller sizes. This occurrence is addressed in the next section. Scores range from 0.2 to 0.95 with an average of 0.52. The three highest ranked craters are crater 6, crater 17, and crater 24, and all are small.

Results from Set B

Because of the high resolution of the MOC imagery and smaller field of view, much of the larger picture and context of the images as they are situated within the craters were lost. Candidates within the initial database are all relatively small, mostly ranging from 10 to 30 km in diameter. To expand this population a second search was completed, this time only by looking at the MOLA base map, which shows a larger regional context. From the second search, 48 additional potential candidates were identified. Candidate craters from set B are larger in size and more similar to the potential candidates identified by Ormö et al. (2004).

High-resolution data (both MOC and THEMIS) were downloaded for the new potential sites (165 images

Table 2. Locations and total scores for all evaluated crater sites within the study area, including those of Ormö et al. (2004), as well as sets A and B.

Set	Crater	Location	Score	Set	Crater	Location	Score
Pilot	A	39°N 11°E	0.50	Set B	41	37°N 9°E	0.55
	B	39°N 11°E	0.60		42	38°N 14°E	0.50
	C	39°N 11°E	0.50		43	38°N 13°E	0.30
	D	39°N 359°E	0.80		44	38°N 10°E	0.40
Set A	1	39°N 4°E	0.60		45	36°N 8°E	0.70
	2	26°N 6°E	0.65		46	34°N 15°E	0.40
	3	34°N 8°E	0.65		47	32°N 14°E	0.60
	5	31°N 17°E	0.40		48	33°N 4°E	0.50
	6	35°N 9°E	0.70		49	36°N 1°E	0.40
	7	35°N 1°E	0.45		50	33°N 1°E	0.40
	8	35°N 3°E	0.50		51	36°N 3°E	0.60
	9	36°N 4°E	0.50		52	40°N 4°E	0.65
	12	35°N 13°E	0.40		53	34°N 355°E	0.45
	14	32°N 11°E	0.30		54	35°N 355°E	0.70
	15	31°N 3°E	0.60		55	36°N 359°E	0.70
	16	33°N 9°E	0.50		56	27°N 13°E	0.55
	17	37°N 6°E	0.70		57	23°N 7°E	0.30
	18	35°N 7°E	0.60		58	27°N 6°E	0.75
	19	39°N 4°E	0.55		60	31°N 351°E	0.30
	24	38°N 354°E	0.95		61	35°N 350°E	0.45
	25	39°N 341°E	0.55		62	35°N 352°E	0.20
	26	40°N 357°E	0.50		64	26°N 348°E	0.55
	27	33°N 357°E	0.40		65	37°N 357°E	0.50
	30	33°N 350°E	0.30		66	38°N 358°E	0.70
	32	37°N 350°E	0.40		68	26°N 346°E	0.40
	35	27°N 14°E	0.30		69	34°N 349°E	0.60
	37	30°N 14°E	0.30		70	31°N 347°E	0.30
	38	30°N 344°E	0.55		72	32°N 346°E	0.20
	40	32°N 4°E	0.60		73	24°N 2°E	0.10
					75	21°N 10°E	0.40
					77	38°N 18°E	0.50
					78	31°N 17°E	0.20
					79	26°N 2°E	0.10
					80	29°N 350°E	0.20
					81	33°N 359°E	0.40
					82	37°N 358°E	0.15
					83	36°N 355°E	0.20
					84	38°N 4°E	0.45
					85	28°N 359°E	0.35
					86	33°N 351°E	0.30
					87	32°N 352°E	0.55
					88	30°N 349°E	0.65
					89	26°N 0°E	0.10
					90	36°N 10°E	0.60
					91	34°N 3°E	0.30
					92	26°N 357°E	0.20
					93	35°N 347°E	0.50
					94	40°N 1°E	0.40

in total). The candidates in the second set were judged by the same system of quantification as those in the first and the results are shown in Fig. 4. From set B there are four small craters (D = 10–30 km), 29 medium craters (D = 30–50 km), and 15 large craters (D = 50–100 km). Total scores range from 0.1 to 0.75 with an average of 0.42. The highest ranked crater is crater 58, with four craters (craters 45, 54, 55, and 66) following

Table 3. Locations and total scores for some crater sites further south west of the study area (outside the proposed shorelines), evaluated on comparison with those that fall within the shorelines.

Crater	Location	Score
1	08.18°N 001.36°E	0.40
2	08.67°N 001.92°E	0.25
3	03.60°N 003.46°E	0.40
4	09.51°N 004.50°E	0.10
5	09.60°N 005.08°E	0.40
6	05.24°N 005.81°E	0.40
7	07.20°N 006.90°E	0.45
8	10.00°N 008.25°E	0.50
9	05.56°N 008.55°E	0.30
10	08.20°N 008.70°E	0.35
11	03.69°N 009.64°E	0.45
12	07.53°N 010.00°E	0.20
13	02.15°N 010.60°E	0.30
14	08.80°N 011.10°E	0.50
15	06.75°N 011.80°E	0.30
16	06.73°N 014.35°E	0.40
17	05.06°N 016.30°E	0.50
18	06.01°N 016.60°E	0.30
19	05.36°N 016.75°E	0.20
20	08.30°N 018.60°E	0.40

closely. Crater 58 is large, but the other four top-rated craters are all medium in size.

The scale of the MOLA imagery and the large sizes of the craters made judging the second set of potential candidates challenging. The regional scale of the imagery means that the resolution is too low to judge individual features such as slumps and flows. In addition, for larger craters only small parts of the crater are covered by a single image, hence entire features cannot be seen and the context of features is lost. Available imagery does not sufficiently cover the potential sites to assign total scores with certainty, and therefore the average total scores are lower for the second set than for the first.

Exemplary Candidates

From the 77 craters in the database, 9 were chosen for further discussion based on ranking. Craters D, 6, 17, 24, 45, 54, 55, 58, and 66 have total scores of 0.7 or higher, and were the highest-ranking examples in this study. Most of these crater sites are discussed in more detail in the next section. All of these craters exhibit signs of slumping, RC, and ST. Furthermore, 77% of these show signs of debris flows and RD, and 66% have RG and/or CT. Pie-charts for the characteristics observed in these craters are drawn in Fig. 5. WMM is divided into two categories: slump (WMM-S) and flow

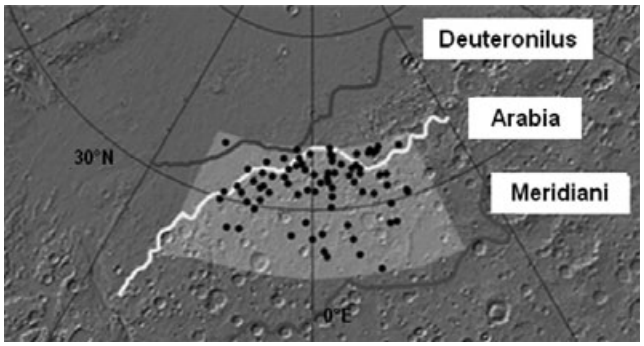

Fig. 3. Locations of all potential shallow marine impact craters of this study in relation to the three shorelines proposed by Parker et al. (1989) as well as Edgett and Parker (1997). Shorelines are labeled, and Meridiani shoreline is shown in light gray, Arabia shoreline is shown in white, and Deuteronilus shoreline is shown in dark gray. North polar projection hill shade base map is from the United States Geological Survey and is based on Mars Orbiter Laser Altimeter topographic data. Study area is indicated by the light gray quadrangle.

(WMM-F). The sizes of the exemplary candidates range from 20 to 60 km in diameter, with most of the craters falling in the medium (30–50 km diameter) range. The average total score for set A is 0.52 ± 0.15; whereas the average total score for set B is 0.42 ± 0.18. Again, total scores within set B are slightly lower than those in set A because of the lower resolution of the MOLA data. The standard deviations for both sets are less than 0.2, indicating a grouping of total scores around the average values.

In impact crater studies, several physical parameters are used to describe impact craters, including the rim diameter and crater depth, two of the most important morphologic elements of an impact crater (Stewart and Valiant 2006; Boyce and Garbeil 2007). The depth to diameter ratio is often a reliable indicator of the type of crater (i.e., the environment in which it was formed) and the extent of crater modification (Garvin et al. 2000; Aharonson et al. 2001; Boyce et al. 2005). Diameter may not change much during crater modification and can be used as a good estimate of original crater size, but in contrast, surface processes significantly influence crater depth over time (Boyce et al. 2005; Stewart and Valiant 2006; Boyce and Garbeil 2007).

Depths, diameters, and depth-diameter relationships were measured in this study. Common depth-diameter ratios for simple, terrestrial craters range from one-third to one-fifth, depending on the nature of the target material (Melosh 1989; Ormö and Lindström 2000). More particularly, $d = 0.29D^{0.93}$ for simple terrestrial craters, and $d = 0.15D^{0.43}$ for complex terrestrial craters (Grieve 1987), where d is the depth of the crater from the rim, and D is the rim-to-rim diameter, both in

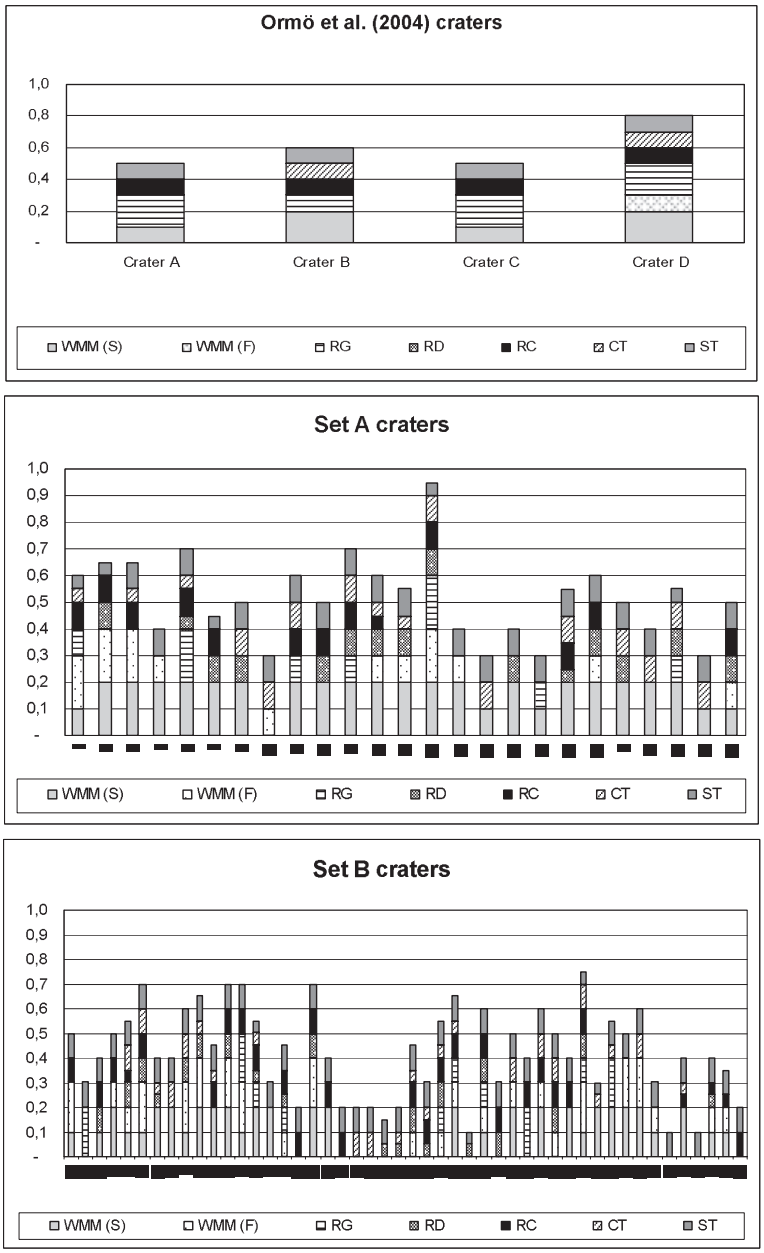

Fig. 4. Stacked columns with individual contributions to the overall ranking or total value for the four candidate Martian marine craters proposed by Ormö et al. (2004), for set A craters, and for set B craters. Wet mass movement is split into two subcategories: slump (S) and flow (F).

km. Notice that complex craters are shallower than simple craters. Although the transition between simple and complex craters on Earth is around 4 km, on Mars it occurs at around 7 km (Garvin et al. 2000). Garvin et al. (2000) found depth-diameter relationships for Martian polar and nonpolar craters to be $d = 0.03D^{1.04}$ and $d = 0.19D^{0.55}$, respectively. For fresh, complex craters on Mars, this relationship has been defined as $d = 0.33D^{0.53}$ (Smith et al. 2001) or $d = 0.381\mathrm{D}^{0.52}$ (Boyce and Garbeil 2007) and ranging from roughly $d = 0.2D^{1.0}$ to roughly $d = 0.5D^{0.25}$ (Stewart and Valiant 2006). Depth-diameter ratios for Martian craters seem to decrease with an increase in latitude because of an increase in subsurface volatiles and ices (Barlow 1993, 1995). Craters in Arabia Terra have a d/D ratio ranging from 0.07 to 0.09 (Barlow 1993, 1995). Modeling experiments suggest that marine target craters should be wider than craters formed on land under similar conditions (Gault and Sonett 1982) because of radial enlargement (Dypvik and Jansa 2003).

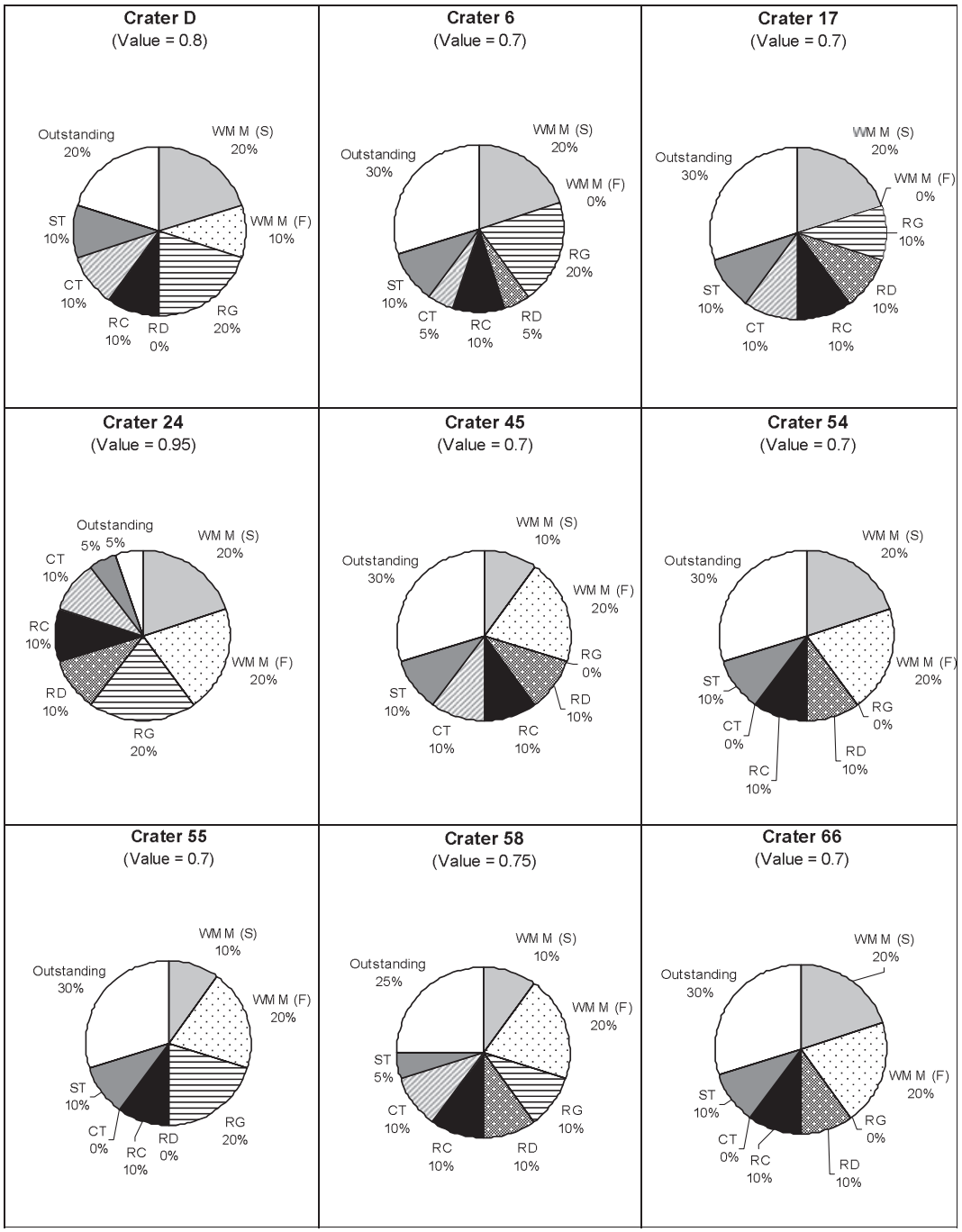

Fig. 5. Breakdown of characteristics present in exemplary candidates. Total values are the sums of the percentages of present characteristics and are shaded or hatched. Outstanding values are the sums of absent characteristics and are shown in white.

Some processes have been suggested to be responsible for the widening of the crater, of which the most common are rim failures as a result of resurge or erosion by water currents or because of sediment instability. Boyce et al. (2005) concluded that the low depth-diameter ratios suggest subsequent infilling by sedimentary deposits, thus supporting the theory of a large ocean depositing the Vastitas Borealis Formation during the Late Hesperian/Early Amazonian.

The accuracy with which these parameters are measured depends directly on the resolution of the MOLA data. Depths were measured by subtracting the average height of the crater floor (dc) from the average height of the crater rim (dr). MOLA topography is not

Table 4. Physical parameters of exemplary candidates, as measured from Mars Orbiter Laser Altimeter data. All depths are negative, or below mean surface level, and the column "ratio" gives the ratio between the measured and predicted depths (see text for further explanation).

Crater	dr (m)	dc (m)	Depth (m)	Diameter (km)	Depth/diameter ratio	Estimated depth (m)	Ratio
D	3599	3746	147	37	0.0040	1384	9
6	2325	2874	549	26	0.0211	1140	2
17	2022	2394	372	23	0.0162	1066	3
24	3698	4375	677	21	0.0322	1014	2
45	2152	2783	631	32	0.0197	1278	2
54	3468	4135	667	36	0.0185	1364	2
55	3411	4155	744	36	0.0207	1364	2
58	1902	3051	1148	60	0.0191	1806	2
66	3642	4387	745	32	0.0233	1278	2

continuous and the use of this data set is prone to errors; however, four measurements were taken on the rim and another four just inside of it and these measurements were averaged to yield the best number. Table 4 lists the depths, diameters, and depth-diameter ratios (*d/D* ratios) as measured and calculated for the exemplary candidates. Note that the *d/D* ratios range from approximately 0.01 to 0.03, which is much lower than the ratios of 0.07 to 0.09 measured for craters in Arabia Terra by Barlow (1993, 1995). Low depth-diameter (*d/D*) ratios could be an indication of age as older craters have rims that have been more eroded and crater shapes that are shallower owing to sediment infilling (Craddock et al. 1997), or it could be a result of the difference in topographic data that was used for the measurements (Viking as opposed to MOLA). However, resurge deposits and postimpact sedimentation from the water column would fill the crater faster than craters on land, and could therefore also be responsible for the low crater depths. Using the depth-diameter relationships defined by Garvin et al. (2000), one can estimate the depth by substituting the diameter (shown in Table 4). Crater D stands out as potentially anomalous with nearly an order of magnitude difference between the measured and the estimated values. The rest of the depths vary consistently with a factor around 2, possibly because of differences in crater populations, for example, faster rates of infilling for craters in shallow marine environments.

Comparative Analysis

As a comparative study, a small area southeast of the study area was selected and 20 craters were evaluated using the similar high resolution THEMIS imagery and the same ranking system. The selected area is located slightly south east of the Arabia Terra study area, within 0°N to 10°N and 0°E to 20°E (Fig. 6). The average total score for this new set is 0.355 ± 0.1. Total scores in the comparative set are lower with almost 20% than those of set A, and with almost 10% than those of set B. Remarkably, the standard deviation is much less than for sets A and B, indicating even more of a grouping of total scores around average values. The highest ranking crater in the comparative group received a score of 0.5. This is quite a high score, and considering that the craters in this comparative area should not have formed under water and should not exhibit shallow marine crater features, it should be noted once more that the characteristics used in our system of evaluation are not absolute and much remains to be discussed. Some features could be the result of other processes, and it is impossible to say with certainty whether certain deposits are truly resurge-related because of the lack of surface geological observations. This is merely the start of a possible way to quantitatively evaluate possible marine impact craters.

INTERPRETATIONS

The shallow marine impact crater candidate database contains the four craters identified by Ormö et al. (2004), 25 craters identified in set A, and 48 craters identified in set B. From this database, nine exemplary candidates were chosen and their locations relative to the proposed shorelines are shown in Fig. 7. In this figure, the dark gray line represents the location of the Deuteronilus shoreline and the light gray line represents the location of the Arabia shoreline. The Meridiani shoreline runs further southeast and all candidate craters fall within its boundaries.

The exemplary candidate craters are divided into three classes based on total scores, sizes, and locations. Three of the nine craters fall into the type I group; a further five fall into the type II group; and one falls within the type III group. There seems to be a direct correlation between location of the crater and its rating.

Type I candidates include well-developed, mostly medium-sized examples and are located in close proximity to the Arabia shoreline; type II candidates include typical, small and medium examples and are located some distance away from the Arabia shoreline, in the direction of the Meridiani shoreline (see Fig. 7). It is impossible to comment on the spatial distribution of type III craters as there is only one large potential candidate. Based on the close proximity of the exemplary candidates to the Arabia shoreline, it seems more likely that this shoreline, instead of the Meridiani shoreline, was in fact the shoreline of an ancient Noachian ocean. However, as the Meridiani shoreline does include all sites, it cannot be excluded as a possible shoreline at some point in Martian history. Additionally, even though most candidate sites fall outside the younger Deuteronilus shoreline, it is still possible that some marine craters may have formed in a more recent oceanic environment.

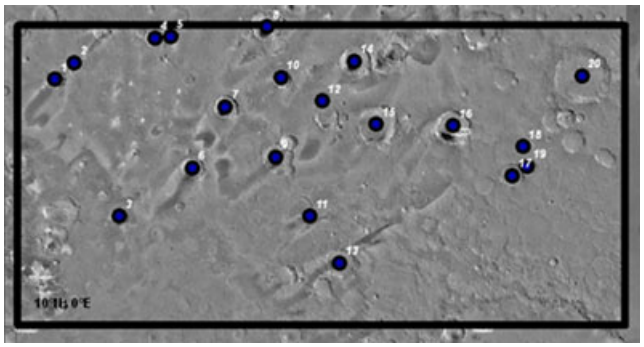

Fig. 6. Locations of comparative craters and their spatial distribution. Study area is located from 10°N, 0°E to 20°N, and 20°E.

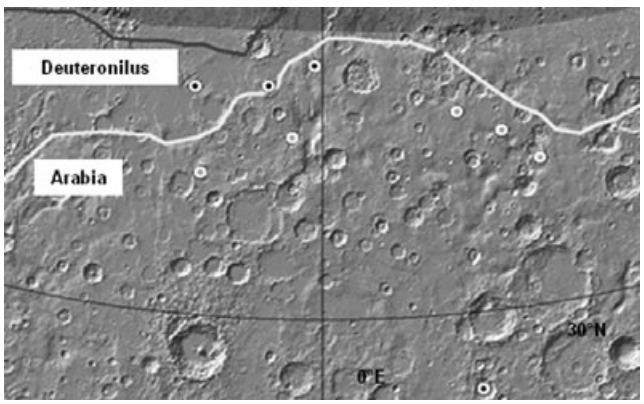

Fig. 7. Locations of exemplary candidate craters and their spatial distribution relative to the Deuteronilus (dark gray) and Arabia (light gray) shorelines. Meridiani shoreline lies toward the southeast. Craters with dark gray dots correspond closely to the Deuteronilus shoreline and those with light gray dots correspond closely to the Arabia shoreline.

Type I Candidates

Crater D

Ormö et al. (2004) originally identified crater D as a potential marine target crater, based on certain morphological features observed by looking at Viking imagery. Crater D is located at roughly 39.0°N and 359.0°E and well within the Meridiani shoreline as defined by Edgett and Parker (1997) and Fairén et al. (2003). Several MOC images draped over a MOLA base map in ArcGIS create a layered, composite, context images with high resolution details. Of the potential marine craters suggested by Ormö et al. (2004), crater D has the highest total score of 0.8. In Fig. 8 (left), the RG are the most remarkable features of this candidate crater (indicated by white dashed lines). One large gully enters the crater from the southwest and is likely responsible for the large resurge deposit (A) located in the southwestern section of the crater. Features of WMM are also evident in both the form of slumping of the crater wall as well as the flow of some debris flows, particularly in the southern part of the rim (B).

Crater D is roughly 37 km in diameter and hence falls in the medium class (30–50 km in diameter). The depths between the surrounding topography and the bottom of the crater floor vary greatly, but average around 200 m. A north–south profile of crater D is shown in Fig. 9a. The *d/D* ratio was calculated to be 0.004, and even though low values are expected for marine craters on Mars, this value could be anomalously low considering that the average *d/D* ratio for the exemplary candidates is 0.02. As mentioned earlier in this article, low *d/D* ratios are indicative of old age and large amounts of sedimentation. Impacts into marine environments should exhibit more sediment infilling than impacts on land. Resurge and tsunami deposits could contribute largely to this rapid infilling; beyond regular fast rates of burial. From the profile shown in Fig. 9a, one can see the terraced central uplift and what seems to be a central ring. The ST of the crater walls is clear on the northern rim. Also visible in the southern half of the profile is a terraced resurge unit, possibly deposited by a large gully entering from the southwest.

Crater 24

Located at roughly 38.4°N and 354.0°E, and well within both the Arabia and Meridiani shorelines, crater 24 has a total score of 0.95—the highest ranking of all craters in the database. This crater exhibits all the characteristics, except that the topography is not as subdued as expected, casting some doubt on the age of this crater. Additionally, the presence of an ejecta

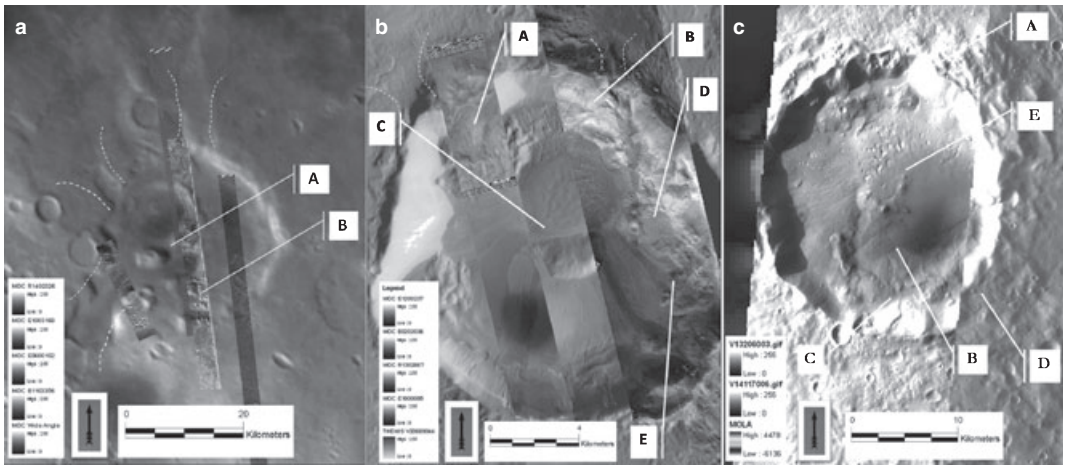

Fig. 8. Examples of type I craters (from left to right). a) Mars Orbital Camera (MOC) narrow angle image overlay in detail for crater D. Radial gullies are indicated by white dashed lines and resurge deposit (A) as well as mass movement deposit (B) are discussed in text. b) MOC narrow angle image overlay in detail for crater 24. Radial gullies are indicated by white dashed lines and resurge deposits (A), slump deposits (B), a central terrace (C), signs of rim collapse (D), and debris flows (E), are indicated by labels. c) Thermal Emission Imaging System image overlay for crater 66. Features A and B are slump and flow deposits, feature C is a collapsed rim, feature D is subdued topography, and feature E is a terraced central pit.

blanket around the crater is indicative of a younger formative age (Barlow 1990). Thus, even though the confidence rating is high, it is arguable that this crater did in fact form during the Noachian. However, because of the relatively close proximity of this crater to the younger Deutoronilus shoreline (of Hesperian age), one cannot exclude its potential marine origin. In terms of morphology, this candidate exhibits some good examples of the characteristics that are thought to be present in shallow marine impact craters (see Fig. 8, middle). Deposits that have a possible resurge origin are the most remarkable features of this candidate crater (A). Gullies seem to enter the crater from the northwest as well as the north-northeast (shown in white dashed lines) and are likely to be responsible for the large RD located in the both these areas. Large amounts of slumping can be seen around the crater rim (B), and although a central terrace is present in this crater (C), large amounts of postimpact sediments seem to cover most of the intracrater terrain. In some places the rim has started to collapse (D). Debris flows dominate the eastern half of the crater (E). Some of the flows, particularly in the south-southeast, are much younger than the crater itself and are the result of subsequent draining into the crater. Large valleys can be seen in the south-southeast and these should not be confused with the flows related to the impact such as those further north.

Crater 24 is roughly 21 km in diameter (the smallest of the exemplary candidates) and hence falls in the small class (10–30 km diameter). A north–south profile of crater 24 is shown in Fig. 9b, from which one can see that this crater is fairly deep and that the rim is still somewhat elevated above the surrounding areas. A thick sedimentary unit is visible in the southern half of the profile, and although it is possibly a resurge unit resulting from the gully to the south-southwest, it is impossible to exclude postimpact sedimentation from younger drainage systems. This resurge unit may be responsible for the low d/D ratio (0.03) calculated for this crater. Regardless of the fact the d/D ratio is low compared with that of other craters on Mars, it is still the highest d/D ratio measured in this study, indicating that this crater may be younger than the other exemplary craters. Again, this may indicate that crater 24 is not of Noachian age, yet it could still be of marine origin and could have formed during the Hesperian period.

Crater 66

Located at roughly 38.2°N and 357.5°E, crater 66 lies within both Arabia and Meridiani shorelines, thus the probability that it was formed in a marine environment is quite high. Crater 66 has a total score of 0.7. Particularly striking in Fig. 8 (right) are the features of WMM. Both slumps and flows are present, particularly near the southern and northern parts of the crater (A and B). This is in agreement with the general location of the crater in relation to the shoreline. According to paleogeography, the resurge waters would have entered the crater from the north and potentially affected the northern walls more severely than the eastern or western walls. The crater's wall has collapsed in the southernmost parts of the crater (C).

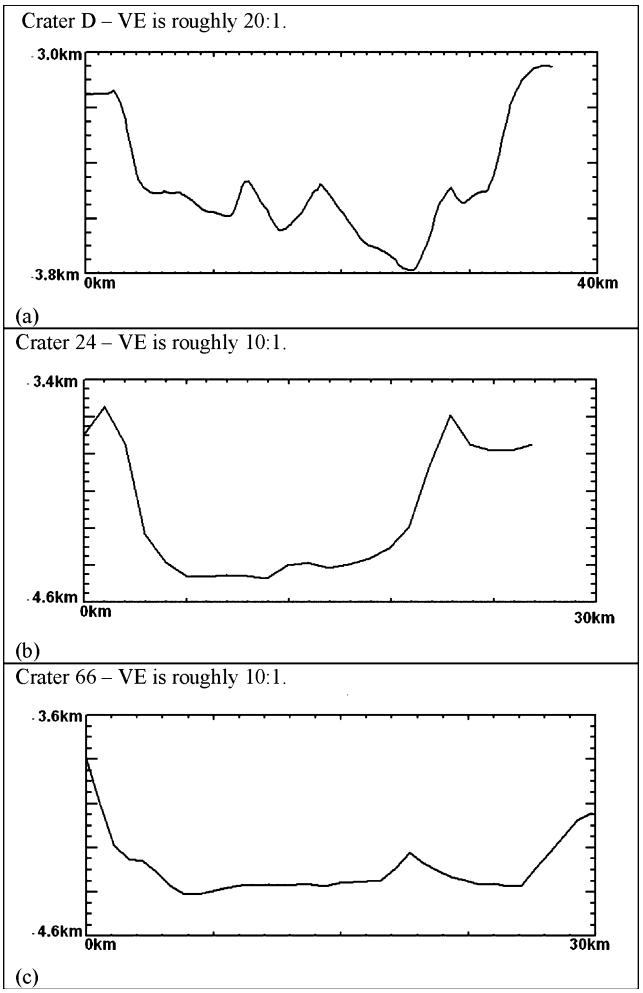

Fig. 9. Profile views of three exemplary candidate craters showing varying depth (in km) with variation in lengths (in km) along a profile from north (left) to south (right).

Topography in and around crater 66 is subdued and the rim is hardly elevated above average surface height (see D in Fig. 8, right). The central pit, likely a summit pit (see Barlow 2009, 2010), seems possibly to have been affected by resurge waters by having the entire northern half obliterated (E). Crater 66 is roughly 32 km in diameter and therefore falls in the medium class (30–50 km diameter). It has a low *d/D* ratio (0.02), which is average for this population of craters. A north–south profile of crater 66 is shown in Fig. 9c, in which slumping is evident, particularly in the northern parts of this crater. A topographic high is visible in the southern half, but this uplift is only the southern part of the eroded central pit. Resurge waters are likely to have completely eroded the northern part of the central pit. The sedimentary deposit directly north of this collapsed central pit could have formed as a result of water resurge from the north, leaving blocks of rim and other material on the crater floor. The location of the gully that may have dumped this sediment is uncertain, but the water may have been too shallow to allow gully formation. Depths between the ST and the bottom of the crater floor vary between 300 m in the south and 600 m in the north. This supports the observation of structural rim failure and ST in the southern crater wall.

Type II Candidates

Crater 6

Crater 6 is located at roughly 35.3°N and 9.2°E and has a total score of 0.7. As seen in Fig. 10 (left), slumping is evident all around the rim (A), but no debris flows are present. The CT is not well developed and may be covered in postimpact sediments. A few small gullies are present (shown with white dashed lines), but they are not distinct and possibly even postimpact. It is mainly the RC sedimentary deposit (B) in the northwest corner of the structure that indicates some resurge.

Crater 6 has a diameter of approximately 26 km and falls in the small class (10–30 km in diameter). The *d/D* ratio for crater 6 is approximately 0.02; around average again for the exemplary candidates. A north–south profile of crater 6 is shown in Fig. 11a, within which the terraced central uplift is the most prominent feature. Large slumps are present in the northern half of the structure and the ST of the crater walls is clear on the southern rim.

Crater 54

Located at roughly 34.9°N and 354.8°E, this crater has a total score of 0.7. Features of WMM are evident in both the form of slumping of the crater wall (A) as well as some of the debris flows (Fig. 10, right). A large well-developed debris flow tongue (B) is visible in the north-northeast of the crater, and numerous smaller flows are also visible in the THEMIS images. Some of these debris flows may be much younger than the crater itself. The crater rim is not elevated above the topography, and in some places, the rim has collapsed (C). No gullies are observed in this crater, and no CT is evident. Some structural blocks are found on the crater floor (D), possibly deposited as rim material being washed into the crater as the water returns.

Crater 54 is 36 km in diameter (very similar to crater D) and hence falls in the medium class (30–50 km diameter). It is also close to crater D in a relative location. A north–south profile of this crater is drawn in Fig. 11b. Depths between the surrounding topography and the bottom of the crater floor vary greatly, with a maximum of 1500 m. The central uplift and ST are the two features that are most evident from

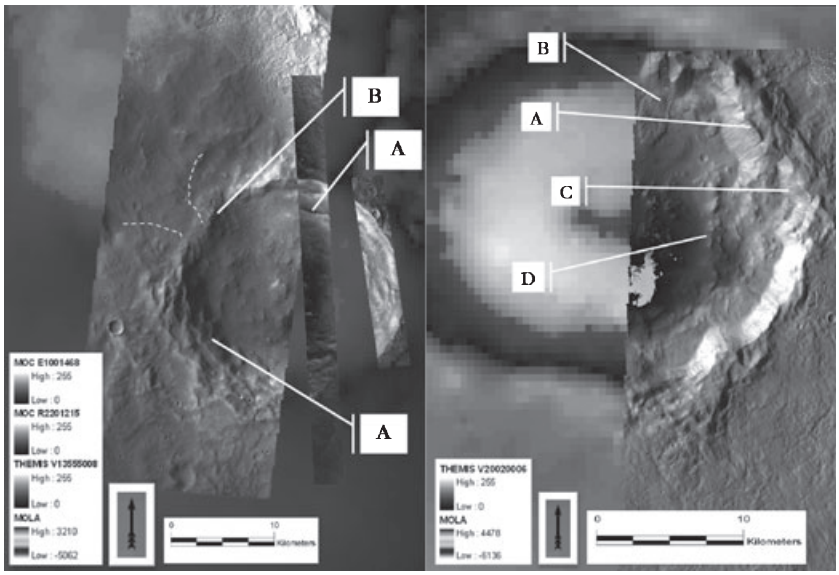

Fig. 10. Examples of type II craters (from left to right). a) Crater 6 compiled from Mars Orbital Camera and Thermal Emission Imaging System (THEMIS) image overlays. Features labeled A are slump deposits and feature labeled B is a possible resurge deposit related to structural rim failure. b) Crater 54 with THEMIS image overlay. Features A and B are slumps and flows, respectively, feature C is a collapsed rim, and feature D refers to structural blocks that could be part of a resurge deposit.

the profile. Some slumping is apparent in the southern rim area and sediment fills the northern half of the crater, possibly induced by debris flow.

Type III Candidates

Crater 58

Located at roughly 27.4°N and 6°E, crater 58 is the farthest south of all of the exemplary candidates. It is in a class of its own because of its large size and because of its relative location to the shorelines and other candidates. It falls within the Meridiani shoreline, but is not even close to the Arabia shoreline, thus decreasing its chances of having formed in an oceanic setting. Crater 58 has a total score of 0.75. Despite its southern location, numerous indicative features are found in this structure. Figure 12 shows the resurge unit that enters the crater structure from the north (labeled A) and that has been subsequently modified and eroded. This is in accordance with the assumed age of the craters in this crater population. RG seem to enter the crater from a few different areas, mainly from the north (shown with white dashed lines). MOLA topography indicates a large low-lying area directly to the north of this crater, and the rim in this vicinity is totally collapsed. RC indicates resurge; and the relative location of the crater with respect to the proposed shorelines makes this a likely scenario. Features of WMM (B) are also present in both the form of slumping of the crater wall as well as debris flows, but these features are not well defined in this crater.

Crater 58 is roughly 60 km in diameter and is the only exemplary candidate that falls in the large class (50–100 km in diameter). A north–south profile of crater 58 is shown in Fig. 11c. From the profile shown in Fig. 11c, one can see possible RD in the northern half of the crater where the rim is largely destroyed. This resurge unit could likely be responsible for the crater's low *d/D* ratio of around 0.02. The topography is subdued, particularly in the north.

Summary

Based on the quantification system designed in this study, nine craters were rated with total scores of 70% or higher and are subsequently classified as exemplary candidates. All these craters exhibit signs of slumping, RC, and ST. Furthermore, 77% of the exemplary candidates show signs of debris flows and RD and 66% have RG and/or CT. Low depth-diameter ratio values were calculated for all the exemplary candidates. The values may be anomalous, but low values are expected for such old craters, and even more so if large amount of resurge deposition filled the crater shortly after formation. In a comparative study of craters in a nearby area, craters were rated with average total scores of 35.5%, indicating that some factors are clearly ambiguous; however, the scores are lower than those for sets A and B and this shows that the morphology of craters inside and outside the proposed shorelines are at least somewhat different.

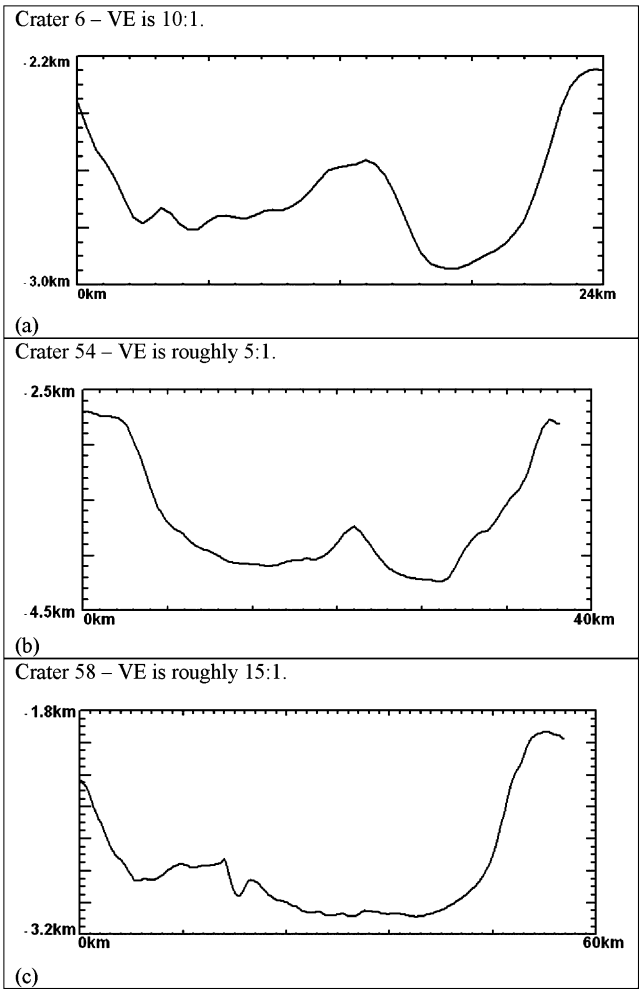

Fig. 11. More profile views of exemplary candidate craters showing varying depth (in km) with variation in length (in km) along a profile from north (left) to south (right).

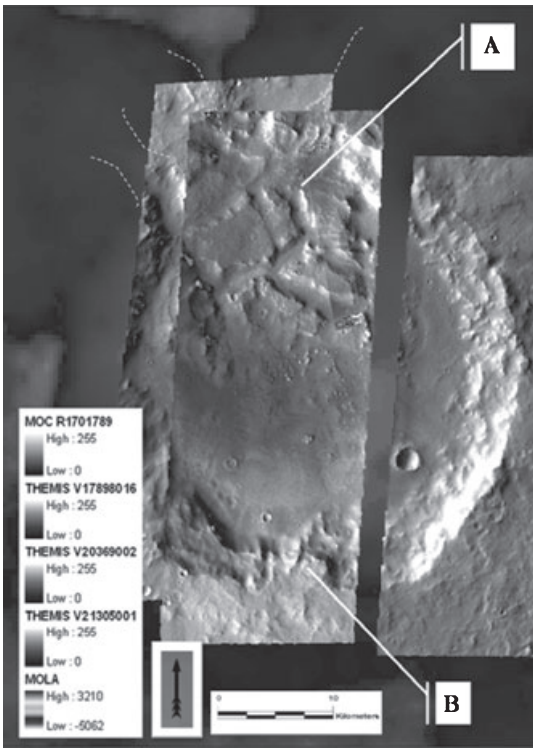

Fig. 12. Example of a type III crater (crater 58) showing Mars Orbital Camera and Thermal Emission Imaging System image overlay on top of Mars Orbiter Laser Altimeter topography. Feature A is an extensive resurge deposit and feature B indicates various wet mass movement deposits. Positions of radial gullies are indicated by white dashed lines.

CONCLUSIONS

This study found 77 impact craters in the area of Arabia Terra on Mars that potentially formed in a shallow marine environment. These craters are identified based on high-resolution imagery data from MOC and THEMIS, in combination with topographic data from MOLA. The classification and ranking of these craters is based on the presence of certain morphological features identified from shallow marine craters on Earth.

The exemplary candidates were classified into three groups or types. Type I includes well-developed, mostly medium-sized examples located close to the Arabia shoreline; type II includes typical small and medium examples located closer to the Meridiani shoreline; and type III includes other large potential candidates. Based on the close proximity of more of the exemplary candidates to the Arabia shoreline, it seems more likely that this shoreline, instead of the Meridiani shoreline, was in fact the shoreline of an ancient Noachian ocean.

The results of this study are useful in helping develop a general classification and characterization of potential marine craters. However, a few limitations should be considered:

- The images either show a large amount of detail with very little context, or good context but little detail.
- Many of the features that have been listed as characteristics of shallow marine impact craters can also be formed in other ways and are therefore not entirely predictive.
- Not much is known about the geomorphology of terrestrial shallow marine impact craters, particularly from a remote sensing point of view, and thus it is hard to compare terrestrial analogs with Martian examples.

This study concludes that some evidence for potential shallow marine impact craters can be found on the surface of Mars as exemplified by Arabia Terra. However, initial comparative studies indicate that

similar characteristics can be observed in craters that were highly likely to be not formed under water, further emphasizing the fact that these features only indicate possible marine origin. Much work remains to be performed on other study areas in and around the dichotomy boundary as well as in other areas where shallow water impact events may have occurred.

Acknowledgments—Alabama Space Grant Consortium funded this study as a master's thesis through NASA's Experimental Program to Stimulate Competitive Research (EPSCoR). The thesis was published by G. de Villiers in December 2007 and is available on the internet at: http://etd.auburn.edu/etd/handle/10415/1343. Authors acknowledge extensive use of MOC and THEMIS images that are available online. The authors thank Sarah Stewart, Nadine Barlow, and an anonymous reviewer for much appreciated, thorough reviews of this article. Special acknowledgment goes to Trent Hare, Arun Kumar Jayakeerthy, Gerard de Villiers, and Filippo Bianchi for fruitful discussions and assistance with data processing.

Editorial Handling—Prof. John Spray

REFERENCES

Aharonson O., Zuber M. T., and Rothman D. H. 2001. Statistics of Mars' topography from the Mars orbiter laser altimeter: Slopes, correlations, and physical models. *Journal of Geophysical Research* 106:723–735.

Artemieva N. A. and Shuvalov V. V. 2002. Shock metamorphism on the ocean floor (numerical simulations). *Deep-Sea Research II* 49:959–968.

Barlow N. G. 1990. Constraint on early events in Martian history as derived from the cratering record. *Journal of Geophysical Research* 95:14191–14201.

Barlow N. G. 1993. Depth-diameter ratios for Martian impact craters: Implications for target properties and episodes of degradation. LPI Technical Report 93-06 Part 1. Houston, Texas: Lunar and Planetary Institute.

Barlow N. G. 1995. The degradation of impact craters in Maja Valles and Arabia, Mars. *Journal of Geophysical Research* 100:23307–23316.

Barlow N. G. 2009. Martian central pit craters: Summary of northern hemisphere results (abstract # 1915). 40th Lunar and Planetary Science Conference. CD-ROM.

Barlow N. G. 2010. Central pit craters: Observations from Mars and Ganymede and implications for formation models. In *Large meteorite impacts and planetary evolution IV*, edited by Gibson R. L. and Reimold W. U. GSA Special Paper. Boulder, Colorado: Geological Society of America. pp. 15–28.

Boyce J. M. and Garbeil H. 2007. Geometric relationships of pristine Martian complex impact craters, and their implications to Mars geologic history. *Geophysical Research Letters* 34, L16201, doi:10.1029/2007GL029731.

Boyce J. M., Mouginis-Mark P., and Garbeil H. 2005. Ancient oceans in the northern lowlands of Mars: Evidence from impact crater depth/diameter relationships. *Journal of Geophysical Research* 110, E03008, doi:10.1029/2004JE002328.

Christensen P. R., Jakosky B. M., Kieffer H. H., Malin M. C., McSween H. Y., Nealson K., Mehall G. L., Silverman S. H., Ferry S., Caplinger M., and Ravine M. 2004. The Thermal Emission Imaging System (THEMIS) for the Mars 2001 Odyssey Mission. *Space Science Reviews* 110:85–130.

Clifford S. M. and Parker T. J. 2001. The evolution of the Martian hydrosphere: Implications for the fate of a primordial ocean and the current state of the northern plains. *Icarus* 154:40–79.

Collins G. S., and Wünneman K. 2005. How big was the Chesapeake Bay impact? Insight from numerical modeling. *Geology* 33:925–928.

Collins G. S., Melosh H. J., Morgan J. V., and Warner M. R. 2002. Hydrocode simulations of Chicxulub crater collapse and peak-ring formation. *Icarus* 157:24–33.

Craddock R. A., Maxwell T. A., and Howard A. D. 1997. Crater morphometry and modification in the Sinus Sabaeus and Margaritifer Sinus regions of Mars. *Journal of Geophysical Research* 102:13321–13340.

von Dalwigk I. and Ormö J. 2001. Formation of resurge gullies at impacts at sea: The Lockne crater, Sweden. *Meteoritics & Planetary Science* 36:359–369.

Dypvik H. and Jansa L. F. 2003. Sedimentary signatures and processes during marine bolide impacts: A review. *Sedimentary Geology* 161:309–337.

Dypvik H., Gudlaugsson S. T., Tsikalas F., Attrep Jr. M., Ferrell Jr. R. E., Krinsley D. H., Mørk A., Faleide J. I., and Nagy J. 1996. Mjølnir structure: An impact crater in the Barents Sea. *Geology* 24:779–782.

Dypvik H., Burchell M. J., and Claeys P. 2004. Impacts into marine and icy environments—A short review. In *Cratering in marine environments and on ice*, edited by Dypvik H., Burchell M. J. and Claeys P. Berlin: Springer-Verlag. pp. 1–20.

Edgett K. S. and Parker T. J. 1997. Water on early Mars: Possible subaqueous sedimentary deposits covering ancient cratered terrain in western Arabia Terra and Sinus Meridiani. *Geophysical Research Letters* 24:2897–2900.

Fairén A. G., Dohm J. M., Baker V. R., de Pablo M. A., Ruiz J., Ferris J. C., and Anderson R. C. 2003. Episodic flood inundations of the northern plains of Mars. *Icarus* 165:53–67.

Fassett C. I. and Head J. W. 2007. Layered mantling deposits in northeast Arabia Terra, Mars: Noachian-Hesperian sedimentation, erosion and terrain inversion. *Journal of Geophysical Research* 112, E08002, doi:10.1029/2006JE002875.

Garvin J. B., Sakimoto S. E. H., Frawley J. J., and Schnetzler C. 2000. North Polar Region craterforms on Mars: Geometric characteristics from the Mars Orbiter Laser Altimeter. *Icarus* 144:329–352.

Gault D. E. and Sonett C. P. 1982. Laboratory simulation of pelagic asteroidal impact: Atmospheric injection, benthic topography and the surface wave radiation field. In *Geological implications of impacts of large asteroids and comets on the Earth*, edited by Silver L. T. and Schultz P. H. GSA Special Paper 190. Boulder, Colorado: Geological Society of America. pp. 69–92.

Gersonde R., Deutsch A., Ivanov B. A., and Kyte F. T. 2002. Oceanic impacts—A growing field of fundamental geoscience. *Deep-Sea Research II* 49:951–957.

Grieve R. A. F. 1987. Terrestrial impact craters. *Annual Review of Earth and Planetary Sciences* 15:245–270.

Gudlaugsson S. T. 1993. Large impact crater in the Barents Sea. *Geology* 21:291–294.

Horton J. W. Jr., Powars D. S., Gohn G. S., and Ormö J. 2005. Chesapeake Bay impact structure: Morphology, crater fill, and relevance for impact processes on Mars (abstract #3024). Workshop on Role of Volatiles and Atmospheres on Martian Impact Craters. Houston, Texas: Lunar and Planetary Institute. CD-ROM.

Horton J. W. Jr., Ormö J., Powars D. S., and Gohn G. S. 2006. Chesapeake Bay impact structure: Morphology, crater fill, and relevance for impact structures on Mars. *Meteoritics & Planetary Science* 41:1613–1624.

Hynek B. M., Phillips R. J., and Arvidson R. E. 2003. Explosive volcanism in the Tharsis region: Global evidence in the Martian geological record. *Journal of Geophysical Research* 108:5111–5127.

Kenkmann T. and Schönian F. 2005. Impact craters on Mars and Earth: Implications by analogy (abstract #3017). 36th Lunar and Planetary Science Conference. CD-ROM.

Kennett J. P. 1982. *Marine geology*. Englewood Cliffs: Prentice-Hall.

King D. T. Jr., Neathery T. L., Petruny L. W., Koeberl C., and Hames W. E. 2002. Shallow-marine impact origin of the Wetumpka structure (Alabama, USA). *Earth and Planetary Science Letters* 202:541–549.

King D. T. Jr., Ormö J., Petruny L. W., and Neathery T. L. 2006. Role of water in the formation of the Late Cretaceous Wetumpka impact structure, inner Gulf Coastal Plain of Alabama, USA. *Meteoritics & Planetary Science* 41:1625–1631.

Kring D. A. 2005. Hypervelocity collisions into continental crust composed of sediments and an underlying crystalline basement: Comparing the Ries (~24 km) and Chicxulub (~180 km) impact craters. *Chemie der Erde* 65:1–46.

Lindström M., Sturkell E. F. F., Ormö J., and Törnberg R. 1996. The Lockne marine impact in the Ordovician of Central Sweden. *Meteoritics & Planetary Science* 31:A80–A81.

Malin M. C., Danielson G. E., Ingersoll A. P., Masursky H., Veverka J., Ravine M. A., and Soulanille T. A. 1992. The Mars Observer Camera. *Journal of Geophysical Research* 97:7699–7718.

Melosh H. J. 1980. Cratering mechanics—Observational, experimental, and theoretical. *Annual Review of Earth and Planetary Sciences* 8:65–93.

Melosh H. J. 1989. *Impact cratering: A geologic process*. New York: Oxford University, 245 p.

Ormö J. and Lindström M. 2000. When a cosmic impact strikes the sea bed. *Geological Magazine* 137:67–80.

Ormö J. and Muinonen P. 2000. Impact craters as indicators for oceanic phases on Mars (abstract #1266). 31st Lunar and Planetary Science Conference. CD-ROM.

Ormö J., Shuvalov V. V., and Lindström M. 2002. Numerical modeling for target water depth estimation of marine target impact craters. *Journal of Geophysical Research* 107:3–11.

Ormö J., Dohm J. M., Ferris J. C., Lepinette A., and Fairén A. G. 2004. Marine-target craters on Mars? An assessment study. *Meteoritics & Planetary Science* 39:333–346.

Ormö J., Sturkell E., and Lindström M. 2007. Sedimentological analysis of resurge deposits at the Lockne and Tvären craters: Clues to flow dynamics. *Meteoritics & Planetary Science* 42:1929–1943.

Parker T. J., Saunders R. S., and Schneeberger D. M. 1989. Transitional morphology in the west Deuteronilus Mensae region of Mars: Implications for modification of the lowland/upland boundary. *Icarus* 82:111–145.

Poag C. W. 1997. The Chesapeake Bay bolide impact: A convulsive event in Atlantic Coastal Plain evolution. *Sedimentary Geology* 108:45–90.

Senft L. E. and Stewart S. T. 2007. Modeling impact cratering in layered surfaces. *Journal of Geophysical Research* 112, E11002, doi:10.1029/2007JE002894.

Smith D. E., Zuber M. T., Frey H. V., Garvin J. B., Head J. W., Muhleman D. O., Pettengill G. H., Phillips R. J., Solomon S. C., Zwally H. J., Banerdt W. B., Duxbury T. C., Golombek M. P., Lemoine F. G., Neumann G. A., Rowlands D. D., Aharonson O., Ford P. G., Ivanov A. B., Johnson C. L., McGovern P. J., Abshire J. B., Afzal R. S., and Sun X. 2001. Mars Orbiter Laser Altimeter: Experiment summary after the first year of global mapping of Mars. *Journal of Geophysical Research* 106: 689–722.

Sonett C. P., Pierce S. J., and Gault D. E. 1991. The oceanic impact of large objects. *Advances in Space Research* 11:77–86.

Stewart S. T. and Valiant G. J. 2006. Martian subsurface properties and crater formation processes inferred from fresh impact crater geometries. *Meteoritics & Planetary Science* 41:1509–1537.

Tanaka K. I., Skinner J. A. Jr, and Hare T. M. 2005. Geologic map of the northern plains of mars. Available online at http://pubs.usgs.gov/sim/2005/2888/.

de Villiers G., King D. T. Jr., and Marzen L. J. 2007. Shallow marine impact craters on Mars? (abstract # 2233). 37th Lunar and Planetary Science Conference. CD-ROM.